Journal of Power Sources 196 (2011) 4003–4011

Contents lists available at ScienceDirect

Journal of Power Sources

journal homepage: www.elsevier.com/locate/jpowsour

Vanadium solid-salt battery: Solid state with two redox couples

Tomoo Yamamura[a,*], Xiongwei Wu[b], Suguru Ohta[a], Kenji Shirasaki[a], Hiroki Sakuraba[a], Isamu Satoh[a], Tatsuo Shikama[a]

[a] Institute for Materials Research, Tohoku University, 2-1-1, Katahira, Aoba, Sendai, Miyagi 980-8577, Japan
[b] School of Chemistry and Chemical Engineering, Central South University, Changsha 410083, China

ARTICLE INFO

Article history:
Received 3 November 2010
Received in revised form 7 December 2010
Accepted 7 December 2010
Available online 22 December 2010

Keywords:
Solid salt battery
High energy density
Hybrid vehicles
Smart grid
Vanadium

ABSTRACT

We present the "vanadium solid-salt battery" (VSSB), which has high energy density, is low cost, is easily recycled, operates at ambient temperature, and has no requirement for special solvents. The VSSB contains two types of vanadium solid salts that are supported on carbon felts with a minimal amount of hydrosulfuric acid added to moisten the ion-exchange membrane. The optimized VSSB shows a cell potential of 1.34 V, excellent reproducibility for charging and discharging for nearly 100 cycles, a high energy efficiency (87%) and a high energy density (77 W h kg^{-1} at 5 mA cm^{-2} using the carbon felt XF208). The energy density is enhanced by 250–350% compared with conventional vanadium redox-flow batteries.

1. Introduction

Recently, secondary batteries have attracted marked interest for use in electric vehicles, such as hybrid and plug-in hybrid vehicles, and "Smart Grid" electricity networks. Because these batteries need to be compact for use in vehicles or houses, the energy density, i.e., the energy stored per unit weight, must be maximized. Therefore, new batteries must be developed [1–3]. At present, lithium-ion and nickel–hydrogen batteries are widely used as power sources because of their large energy densities (approximately 100 W h kg^{-1}). However, lithium-ion batteries exhibit substantial disadvantages including (i) an uneven distribution of lithium resources in the world [4], (ii) poor environmental friendliness and safety because of the use of flammable organic electrolytes, which are potentially harmful in the case of an accident [5], and (iii) insufficient energy density for batteries in future hybrid vehicles and Smart Grid networks. Concerning inflammability, aqueous batteries such as the lead acid battery and vanadium redox-flow battery (VRFB) are advantageous; however, both possess low energy density and the former contains lead, which is toxic. The VRFB uses only vanadium [6,7], which leads to unique advantages that have been investigated in basic research [8–10] and in applications [11,12]. The fatal disadvantage of the VRFB is that the energy density is as low as 25–35 W h kg^{-1} [13], which is insufficient to meet the demands of electric vehicles and other mobile applications.

To satisfy the above-mentioned conditions (i)–(iii), we propose the new "vanadium solid-salt battery" (VSSB). The VSSB contains VOA_{2/n_A} and VA_{3/n_A} (A: counteranion with a charge of $-n_A$) in the positive and negative electrode composites, respectively, in the discharged state. Because the active materials are solid salts, the energy density is expected to be high. The energy density of the VSSB is moderate (approximately 80 W h kg^{-1}) because of the cell voltage of 1.3–1.4 V and weight of inactive components (i.e., sulfate anion and hydrated water). The use of vanadium is advantageous to the energy density because of its abundance in the earth's crust [14]; it is the 13th most abundant atom, but the eighth most abundant of the lighter elements and fourth most abundant transition element. In addition, there is an even distribution of vanadium resources in the world [4] compared with lithium. Also, by eliminating the inactive parts, the VSSB can be adapted into a vanadium solid oxide battery (VSEB) with much higher energy density.

Because the VSSB is solid, the operating conditions, especially the current density, differ from those of a liquid battery such as a VRFB [15]. Recent developments of solid materials such as carbon materials [16–21] and ion-exchange membranes [22,23] will allow further development of VSSBs. In this paper, the charging and discharging performance of a VSSB is demonstrated, where the counteranion (A) is a sulfate ion (SO_4^{2-}; $-n_A = -2$). This solid battery requires only an aliquot of acid for the membrane to function. A variety of parameters need to be characterized before evaluation of the battery performance. First, the optimal conditions for stable charging and discharging cycles (Section 3.1), membrane and electrode-active materials (Sections 3.2 and 3.3), and operation (Section 3.4) are established. Second, during investigation of

* Corresponding author. Tel.: +81 22 215 2120; fax: +81 22 215 2121.
E-mail address: yamamura@imr.tohoku.ac.jp (T. Yamamura).

0378-7753/$ – see front matter © 2011 Elsevier B.V. All rights reserved.
doi:10.1016/j.jpowsour.2010.12.010

the amount of active material and sulfuric acid required, the mechanisms behind the operation of the VSSB are discussed (Section 3.5). Finally, the theoretical limits of the VSSB are discussed with relation to the results obtained in this study.

2. Experimental

2.1. Structure of the VSSB

A schematic of a VSSB is shown in Fig. 1 and the typical specifications of the cell used in this paper are shown in Table 1. A glassy carbon disc (Tokai Carbon, Japan) of Φ 30 × t 3.0 was used as an electricity collector. The typical amount of active material mixed with carbon felt was 99.4 mg for $V(SO_4)_{1.5}{\cdot}x_3H_2O$ (x_3 = 8.15) and 70.8 mg for $VOSO_4{\cdot}x_4H_2O$ (x_4 = 3.75), where the determination of x_3 and x_4 will be described in Section 2.2. For calculation of the energy density of the battery, only the weights of the active materials were considered, because the objective was to reveal the basic performance compared with the theoretical one, and not to optimize other components such as the carbon electrodes, membranes and cell packaging. For a separator membrane in the cell, a cation-exchange membrane of Neosepta CMX C-1000 (abbreviated as "C-N"), anion-exchange membranes of Neosepta AMX A-9485 (abbreviated as "A-N") and Selemion APS (abbreviated as "A-S") were supplied by Asahi Glass Co., Ltd., Japan. The membranes were immersed in the 2 mol dm^{-3} H_2SO_4. They were then placed in the cell after the excess liquid was removed. Carbon felts (XF208, XF23A, XF30A, and XF30ADP14) were supplied by Toyobo Co., Ltd., Japan. The specific surface areas of the carbon felts were determined by averaging three BET (Brunauer–Emmet–Teller) adsorption measurements (one-point method) obtained using a FlowSorb III 2305 surface-area analyzer (Shimadzu Corp., Japan). Three types of cells, A, B and C, with different electrode area and/or thickness were prepared. The geometrical areas of cells A, B and C were 2.35, 2.35 and 1.17 cm^2, respectively, and the thicknesses were 3.0, 1.5 and 3.0 mm, respectively.

2.2. Preparation of the electrode composite

Oxovanadium(IV) sulfate, $VOSO_4{\cdot}x_4H_2O$, was purchased from Wako Pure Chemical Industries, Japan. A solution of $VOSO_4$ (2 mol dm^{-3}, 50 mL) in aqueous sulfuric acid (2 mol dm^{-3}) was electrochemically reduced on a mercury cathode under a constant current of 1 A using a galvanostat (HA-501, Hokuto Denko Co., Ltd., Japan). The aqueous solution was exposed to air overnight and then the excess sulfuric acid was removed by evaporation for a few days to prepare the $V(SO_4)_{1.5}{\cdot}x_3H_2O$ solid (Fig. 2). The hydration numbers of the salts were determined to be x_3 = 8.15, and x_4 = 3.75 by dissolving a known weight of each salt in water and then determining the concentration of vanadium by inductively coupled plasma atomic emission spectroscopy (ICP-AES). The pentavalent salt $VO_2(SO_4)_{0.5}{\cdot}x_5H_2O$ and divalent salt $VSO_4{\cdot}x_2H_2O$ were prepared by electrolytic oxidation of the tetravalent salt, and electrolytic reduction from the trivalent salt, respectively (Fig. 2).

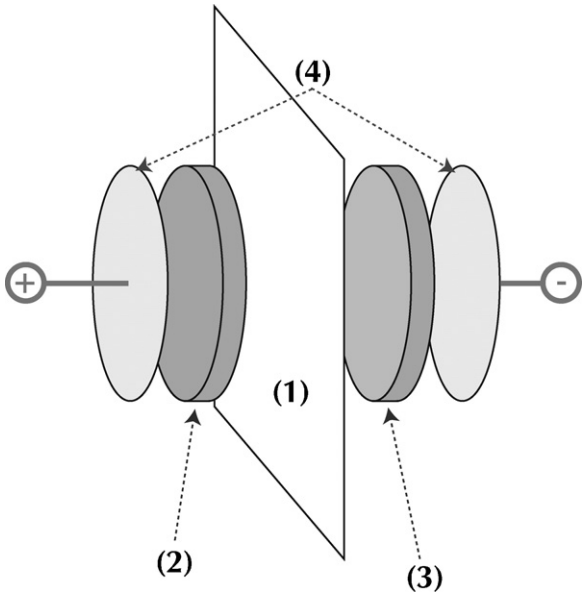

Fig. 1. Schematic of a VSSB: (1) ion exchange membrane, (2) carbon felt electrode supporting $VOSO_4{\cdot}x_4H_2O$, (3) carbon felt electrode supporting $V(SO_4)_{1.5}{\cdot}x_3H_2O$, and (4) glassy carbon electrode.

Supporting the active materials on the carbon felt was performed in two ways. One method simply involves spreading a paste of the active materials on the carbon felt (method 1, Fig. 3). Another technique involves adsorbing the active material onto the carbon felt by soaking the felt in a solution of the active material followed by vacuum drying (method 2, Fig. 3).

2.3. Measurement of charging and discharging performance

The charging and discharging performance of the cells was evaluated using a battery testing system (PFX2011, Kikusui Corp., Japan) under a constant current density of 2, 5, 10, 15, or 20 mA cm^{-2}. The terminal voltage during charging and discharging was recorded every 30 s. Charging was terminated when the terminal voltage reached to 1.80 V, and then charging was terminated at a cutoff voltage E_{CO} of 0.70, 1.0 or 1.3 V. The intermission between the discharging and discharging states and *vice versa*, known as the open circuit voltage, was recorded for 1 minute.

Table 1
Typical specifications of the optimized VSSB cell (sulfate salt system).

Category	Section where variation tested	Item	Typical setting
Performance	3.1	Cell voltage (V)	1.34
		Energy density (W h kg^{-1})	70
Membrane	3.2	Ion exchange membrane	Neosepta CMX C-1000
Electrode-active material composite	3.3	Carbon felt	XF30ADP14, 3.8 mm
		Geometric area (cm^2)	2.35
		Thickness of half cell (mm)	3.0
		Supporting method	Method 2 (See text)
	3.5	Amount of $V(SO_4)_{1.5}{\cdot}x_3H_2O$ in negative side (mol)	1.5×10^{-4}
		Amount of $VOSO_4{\cdot}x_4H_2O$ in negative side (mol)	3.0×10^{-4}
		Concentration and volume of H_2SO_4 added	2 mol dm^{-3}, 0.1 cm^3
Operation	3.4	Current density (mA cm^{-2})	5
		Cut-off voltage (E_{CO}) (V)	0.7

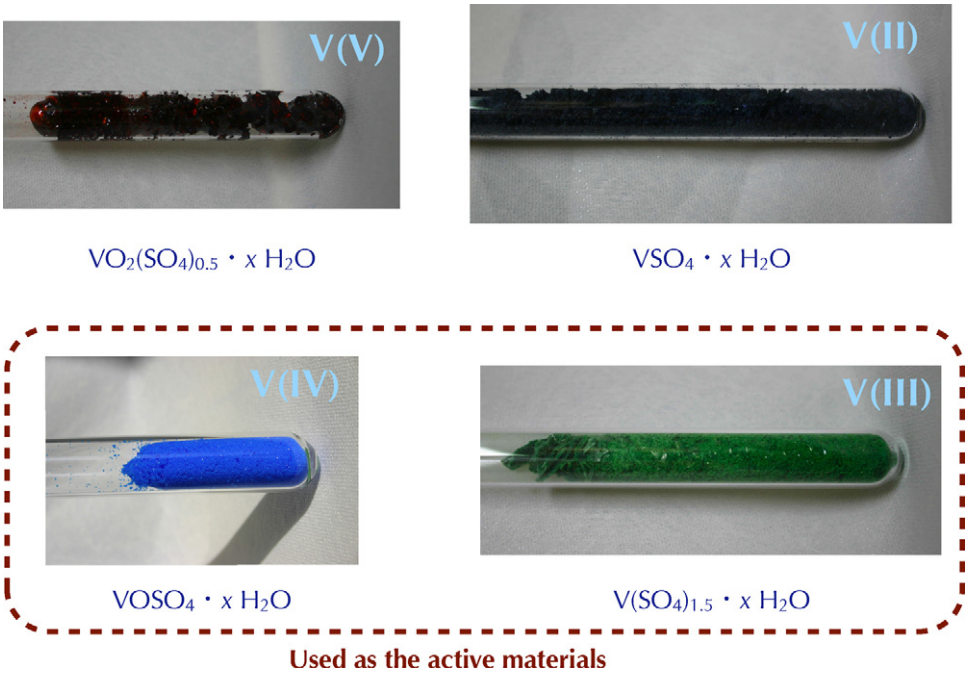

Fig. 2. Photographs of vanadium sulfate salts in various oxidation states.

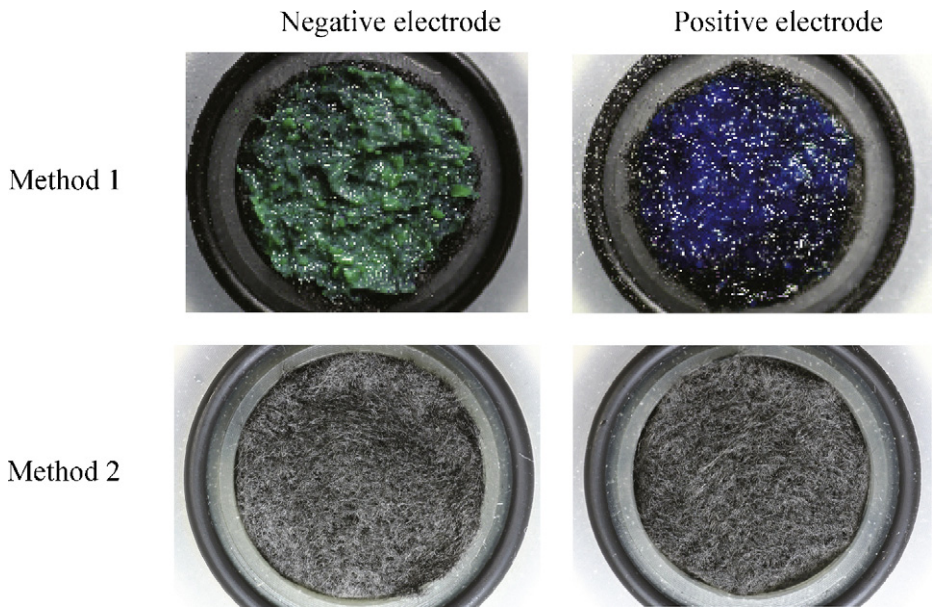

Fig. 3. Images of carbon-felt electrodes containing the active materials for the positive and negative sides of the VSSB.

3. Results and discussion

3.1. Cell voltage and cycling performance

3.1.1. Cell voltage

The obtained charging and discharging curves reveal the excellent performance of the cell, with symmetric and reproducible shapes up to 90 cycles (Fig. 4). The terminal voltage at a current density j is given by:

$$E(j) = \Delta E^0 + \frac{RT}{zF} \ln K \pm \eta \quad (1)$$

where ΔE^0 is the difference in the reduction potentials of the positive and negative reactions, η is the sum of the overvoltage and internal resistance, where η is positive for charging and negative for discharging. The terminal voltage at the intermediate points of charging and discharging (corresponding to $K = 1$) in the second cycle are 1.38 and 1.30 V, respectively. The average of the two voltages, identical to ΔE^0, is 1.34 V, which is similar to the 1.3–1.5 V of a VRFB [15,24,25]. A relatively small overvoltage including an internal resistance of $\eta = 40$ mV also contributed the excellent performance of the cell with symmetric charging and discharging curves.

3.1.2. Cycling performance

Fig. 5 shows typical plots of the energy efficiency (EE), coulombic efficiency (CE) and energy density as a function of the cycle number for the cell. EE and CE decreased significantly between the

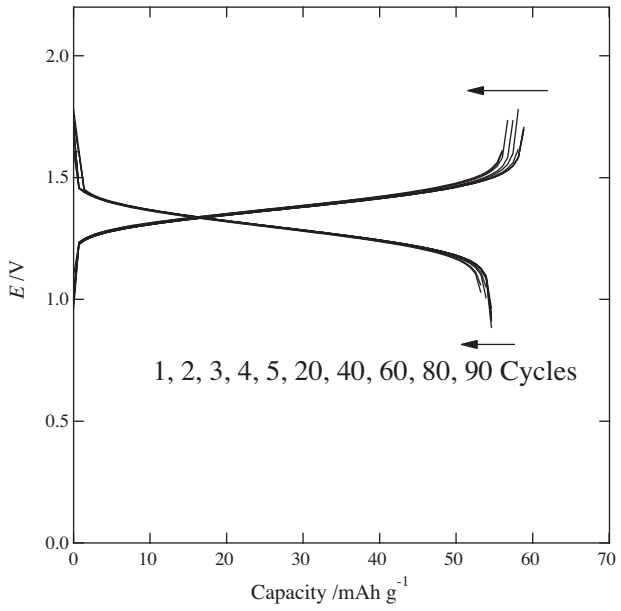

Fig. 4. Charging and discharging curves of a VSSB for 1, 2, 3, 4, 5, 20, 40, 60, 80, and 90 cycles at a current density of 5 mA cm^{-2}.

first and second cycles, and then increased gradually from the second to the 96th cycle (Fig. 5a). The observed singularity of the first cycle can be understood as the attainment of steady state. Therefore, the first cycle was excluded from the statistical evaluation of the EE and energy density. EE and the energy density remained almost constant and the average values from the second to the 96th cycle were 87% and 69 W h kg^{-1}, respectively. These values are much higher than those of 80% and 15–25 W h kg^{-1} [13] for a VRFB.

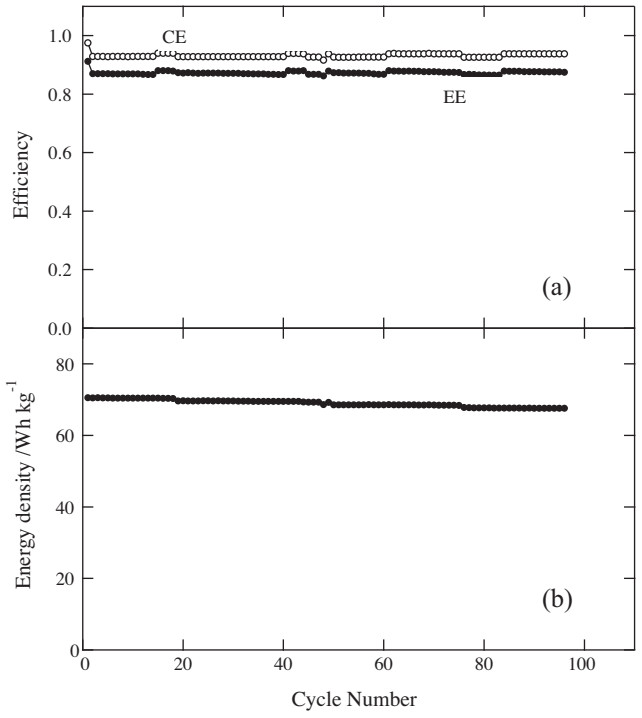

Fig. 5. Plots of (a) energy and coulombic efficiency and (b) energy density of a VSSB as a function of cycle number at a current density of 5 mA cm^{-2}.

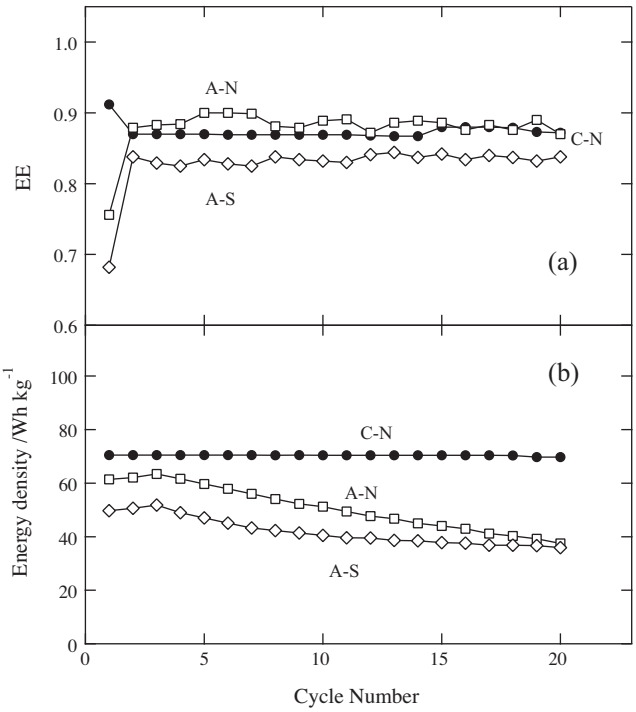

Fig. 6. Dependence of (a) energy efficiency and (b) energy density of a VSSB on the type of membrane. Electrode: XF30ADP14, 3.8 mm thick; geometric area: 2.35 cm^2; supporting method: 2; amount of both active materials: 4.6×10^{-4} mol; operation: current density of 5 mA cm^{-2}; E_{CO} = 0.7 V.

3.2. Membrane

To select the optimal membrane, the EE and energy density at each cycle for 20 cycles were obtained using different membranes (membranes C-N, A-N, A-S), as depicted in Fig. 6 and summarized in Table 2. The battery containing the anion-exchange membrane A-N yielded the highest EE of 88%, although the energy density of this battery decreases with further cycles after the maximum in the third cycle. A similar decrease in the energy density with increasing cycle number was observed for the A-S membrane. The decreasing energy density with high constant EE is a result of the decreasing capacity of the battery as the cycle number increases. The striking deterioration in the capacity of the battery containing the anionic exchange membranes was attributed to the permeability of the anions through the membrane, which leads to mutual contamination of the active material. The cation membrane C-N gave a high EE, which is in contrast to a VRFB where an anionic exchange membrane should be used for suppressing mutual contamination. This means that (i) protons pass through the membrane exclusively in the VSSB, and/or (ii) the active materials exist as anions or as a solid at high concentration. The effect of the high concentration in the VSSB may arise from coordination of vanadium cations with sulfate anions. From these results, the cation membrane C-N gave the highest energy density for the VSSB.

Previous studies [26,27] showed that commercial ion exchange membranes including Selemion (Asahi Glass Co., Japan), and Dow (Dow Chemical Co., USA) are unsuitable for VRFB application because highly oxidizing pentavalent vanadium ions caused their oxidative decomposition. The EE of VRFBs based on a Nafion 117 membrane is 85% and that based on a modified Nafion membrane is 85% [28]. An EE of 87% is higher than those of VRFBs containing Nafion 117 or other improved membranes. This result suggests that oxidation of the membrane is not a serious problem in the VSSB.

Table 2
Energy efficiencies and energy densities of VSSBs containing various membranes at 5 mA cm^{-2}.

Membrane	Abbreviation	Type	Ion exchange capacity[a] (mequiv. g-dry^{-1})	Permselectivity[a] (%)	Resistance[a] (Ω cm^2)	Thickness[a] (μm)	Coulombic efficiency[b] (%)	Energy efficiency[b] (%)	Energy density[b] (W h kg^{-1})
Neosepta CMX C-1000	C-N	Cation	1.62	99	2.91	164	93 ± 0	87 ± 0	70 ± 0
Neosepta AMX A-9485	A-N	Anion	1.25	90.7	2.35	134	96 ± 1	88 ± 0	ND[c]
Selemion APS	A-S	Anion	0.29	88.4	0.68	138	87 ± 1	83 ± 0	ND[c]

[a] Data supplied by manufacturer.
[b] Average of the second to the 20th cycle.
[c] Value was not determined because it shows a maximum value in the third cycle and then decreases with increasing cycle number.

3.3. Solid salt–carbon felt composites

3.3.1. Electrode materials

As seen in Table 3, the carbon felt material affected the EE to a small extent ($\Delta \approx 3\%$), but significantly changed the energy density (by ≈10 W h kg^{-1}). Higher energy densities were obtained for carbon felts XF208, XF23A, XF30A and XF30ADP14 because of their conducting nature. The highest EE of 87% and a high energy density of 70 W h kg^{-1} were achieved for the electrode containing XF30ADP14 at a current density of 5 mA cm^{-2}. XF208 gave an EE and energy density of 83% and 77 W h kg^{-1}, respectively. XF208 gave the largest energy density because it possesses the largest specific surface area of the felts tested (Table 3). In this work, XF30ADP14 was selected for use as the default carbon felt and was used in subsequent experiments.

3.3.2. Dimensions of the VSSB

The EE and energy density for cells A, B and C containing identical amounts of the active material and various dimensions were investigated. The difference in the CE and EE was not significant for different cell structures, i.e., the average values were 87% (EE) and 93% (CE) for cell A; 86% (EE) and 90% (CE) for cell B; and 85% (EE) and 92% (CE) for cell C. However, a distinct difference lies in the energy density of the cell; values of 70 and 65 W h kg^{-1} were obtained for cells A and C, respectively, whereas a significantly smaller value of 38 W h kg^{-1} was observed for cell B. On the basis of the equivalence in the cell dimensions of A and C and their difference to B, it is concluded that the thickness of the electrode composite affects the energy density. This may be connected to the density of the carbon felt: the carbon felt that is 3.8 mm thick would be compressed significantly in cell B (1.5 mm depth) but not in cells A and C (3.0 mm depth). This may change the effectiveness of the active materials because the extensive compression may result in the lack of a diffusion path. In contrast, the energy density of cells A and C shows only a slight difference with different geometric area (2.35 and 1.17 cm^2). This indicates that the electrode area is not an important factor controlling the energy density, which seems intuitive because the energy density can also be designed to be used per unit geometric area.

Of these cells, A shows the highest EE and energy density compared with cells B and C. Therefore, cell A was used as the standard structure hereafter.

3.3.3. Methods for supporting the active materials

The dependence of EE and energy density on the method used to support the active material is depicted in Fig. 7. The EE obtained from cells fabricated using method 2 is almost constant (87%), whereas that obtained using method 1 fluctuated greatly (Fig. 7a). In contrast, the energy density shows a marked difference; the energy density for the VSSB fabricated using method 2 (70 W h kg^{-1}) was superior to that obtained for the cell produced *via* method 1 (Fig. 7b) (method 1, EE: 84, method 2, EE: 87). The energy density remained constant for the cell made using method 2, whereas a gradual deterioration from 36.6 to 29.4 W h kg^{-1} from the eighth to cycle 20 was observed for the VSSB fabricated using method 1. Therefore, method 2 was adopted as the default method for immobilizing the active material on the carbon felt in the VSSBs.

3.4. Operating conditions

3.4.1. Current density

The dependence of EE and energy density on current density was evaluated by averaging the values obtained from the second to the fifth cycles is depicted in Fig. 8. CE increases from 85 to 100%, whereas EE decreases from 86% to 77% when the current density increases from 2 to 20 mA cm^{-2} (Fig. 8a). A negative correlation

Table 3
Energy efficiencies and energy densities of VSSBs containing various carbon felts at 5 mA cm^{-2}.

Carbon felt	Characteristics	Specific surface area[a] ($m^2\ g^{-1}$)	Thickness (mm)	Weight used as electrode[b] (mg)	Coulombic efficiency[c] (%)	Energy efficiency[c] (%)	Energy density[c] ($W\ h\ kg^{-1}$)
XF208	Basic	29	3.3	47	91	83	77
XF23A	Conducting	1.4	3.5	64	90	75	67
XF30A		5.6	4.2	79	93	86	72
XF30ADP14	Conducting and high through-flow	4.8	3.8	85	93	87	70

[a] Average of three measurements.
[b] Weight of one side.
[c] Average of the second to the 10th cycle.

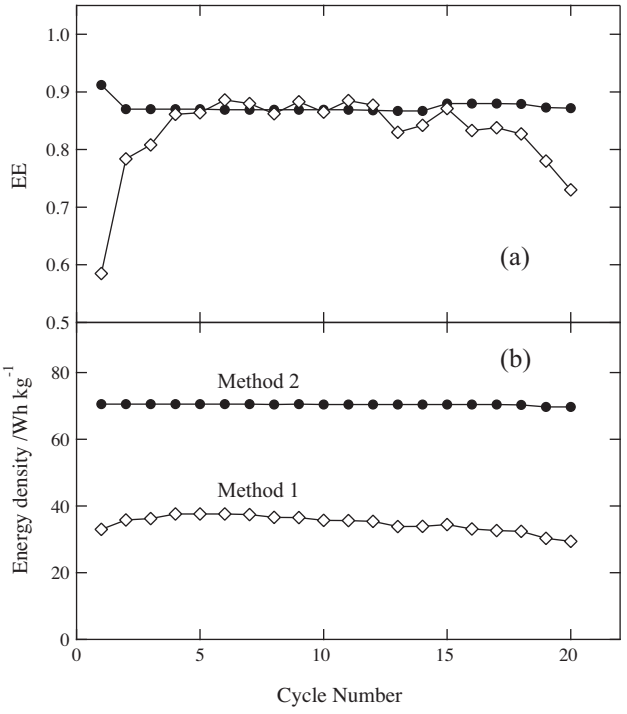

Fig. 7. Dependence of (a) energy efficiency and (b) energy density of a VSSB on the supporting method used to attach the active materials to the carbon felt electrode. Membrane: CMX C-1000; electrode: XF30ADP14; geometric area: 2.35 cm^2; amount of both active materials: 4.6×10^{-4} mol; operation: current density of 5 mA cm^{-2}; E_{CO} = 0.7 V.

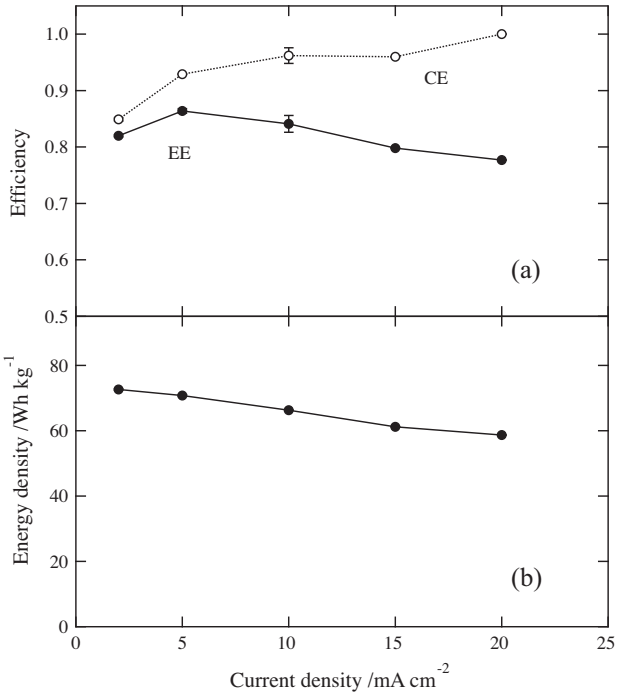

Fig. 8. Dependence of (a) energy and coulombic efficiency and (b) energy density of a VSSB on current density. Membrane: CMX C-1000; electrode: XF30ADP14; geometric area: 2.35 cm^2; supporting method: 2; operation: E_{CO} = 0.7 V. Error bars show one standard deviation.

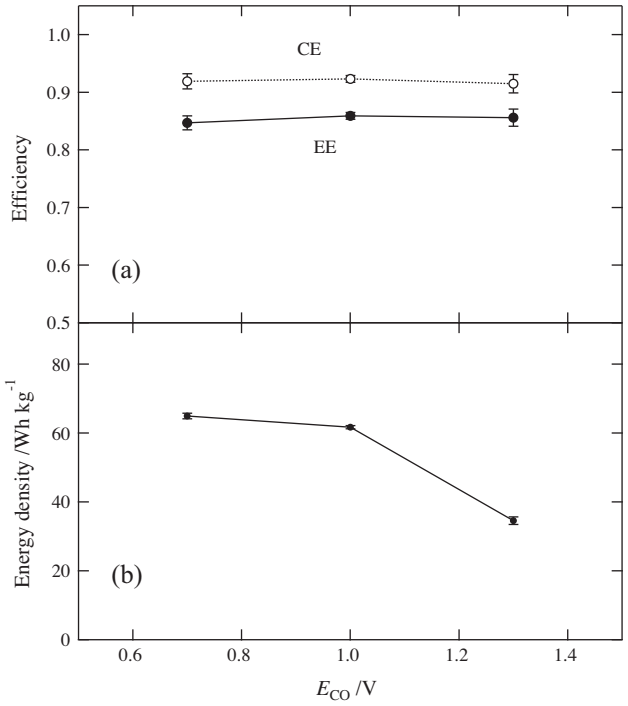

Fig. 9. Dependence of (a) energy and coulombic efficiency and (b) energy density of a VSSB on the cut-off voltage E_{CO}. Membrane: CMX C-1000; electrode: XF30ADP14; geometric area: 2.35 cm^2; supporting method: 2; operation: current density of 5 mA cm^{-2}; E_{CO} = 0.7 V. Error bars show one standard deviation.

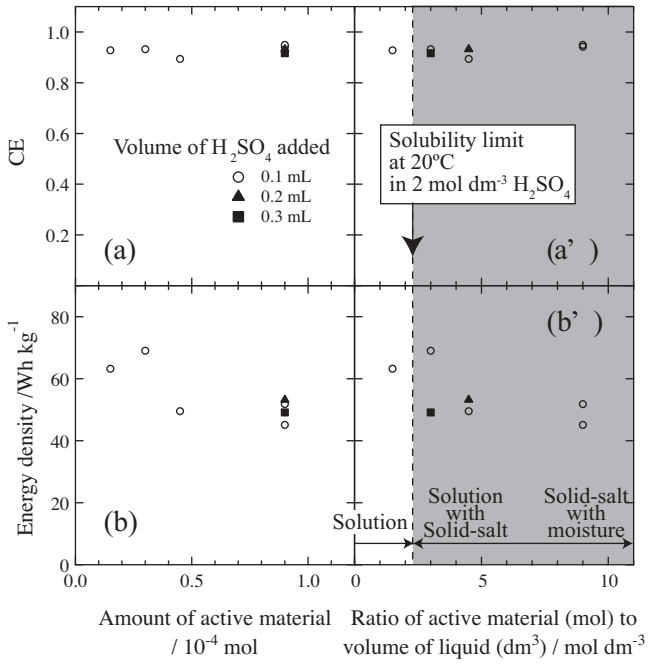

Fig. 10. Dependence of coulombic efficiency and energy density of a VSSB on the amount of active material (a and b). The dependence is also shown against the ratio of active material to the volume of liquid (a′ and b′); the value can be considered a concentration (mol dm^{-3}) if all of the material is dissolved. The shaded area corresponds to above the solubility limit of $VOSO_4$ in 2 mol dm^{-3} H_2SO_4 at 20 °C. Membrane: CMX C-1000; electrode: XF30ADP14; geometric area: 2.35 cm^2; supporting method: 2; operation: current density of 5 mA cm^{-2}; E_{CO} = 0.7 V.

between the EE and current density was first reported by Sun and Skyllas-Kazacos [29,30]. EE deceased from 88.6% (25 mA cm^{-2}) to 84.3% (40 mA cm^{-2}) to 79.0% (60 mA cm^{-2}) as the current density was increased [30]. Because the VSSB is solid, the operating conditions, especially the current density, differ from those of a liquid battery such as a VRFB [15]. The energy density decreases almost linearly from 73 to 59 W h kg^{-1} when the current density increases from 2 to 20 mA cm^{-2} (Fig. 8b). Although the highest energy density was obtained at a current density of 2 mA cm^{-2}, a default current density of 5 mA cm^{-2} was used. Nafion 117 showed an EE of 73–74% at 20 mA cm^{-2}, whereas PVDF-g-PSSA-22, which was prepared by a solution-grafting method, gave an EE of over 75% [31].

3.4.2. Cut-off voltage (E_{CO})

The depth of discharging as well as that of charging affects the performance of a battery. The depth of discharging was changed by applying various E_{CO}, whereas the depth of charging was kept constant (1.8 V). Fig. 9 shows the dependence of EE and energy density on E_{CO}. The EE is constant (85–86%) over 20 cycles at E_{CO} of 0.7–1.3 V (Fig. 9a), whereas the energy density decreases significantly from 62 to 35 W h kg^{-1} when E_{CO} increases from 1.0 to 1.3 V (Fig. 9b).

3.5. Reaction mechanism and theoretical energy density

3.5.1. Amount of sulfuric acid in relation to the solubility limit

When the amount of solid salt increases, the moderate decrease observed in the energy density (*ca.* 70–50 W h kg^{-1}) shows that a decreasing proportion of the solid salt functions effectively in the VSSB (Fig. 10a and b). The lower effectiveness in the case of an increased amount of solid salt may be associated with the stacking of the thin-layered composite electrode to obtain the desired cell voltage and energy density. This finding may correspond to one or both of the following: (1) only part of the active material is active, because only the active material supported in the proximity of the carbon felt functions appropriately; (2) only part of the active material dissolved in solution is active. The same data are plotted as the ratio of active material to the volume of liquid (Fig. 10a′ and b′), giving the concentration if all of the material is dissolved.

The VSSB was equipped with ion-exchange membranes that require moisture for conductivity. The optimum amount of sulfuric acid required for the battery was investigated with careful reference to the solubility of vanadium sulfate in sulfuric acid. The reported solubility of vanadium sulfate was limited: $[VOSO_4]$ = 3.28 mol dm^{-3} in water and $[VOSO_4]$ = 1.786 mol dm^{-3} in 3 mol dm^{-3} H_2SO_4 at 20 °C [32]. The smooth decrease in the solubility of vanadium sulfate with the concentration of acid enables us to extrapolate a theoretical solubility of 2.28 mol dm^{-3} in 2 mol dm^{-3} H_2SO_4 at 20 °C. The CE and energy density of a cell containing this amount of sulfuric acid were plotted. The shadowed region indicates that part of the active material does not dissolve due to the limited solubility of vanadium sulfate in H_2SO_4. The data in Fig. 10b′ indicate that the battery works with the major part of the active materials present as a solid.

3.5.2. Reaction mechanism

As revealed in Section 3.5.1, the VSSB functions with mostly solid salts. This shows that the redox reaction including dissolution and solidification processes proceeds with very low overvoltage. The redox reactions on the positive and negative composite electrodes are considered to occur as shown in (2) and (3), respectively.

$$VO_2A_{1/n_A}\cdot x_5H_2O \overset{\text{dissolution}}{\underset{\text{solidification}}{\rightleftarrows}} [VO_2A_{n_5/n_A}(H_2O)_{m_5}]^{(1-n_5)+} \overset{+e^-}{\underset{-e^-}{\rightleftarrows}} \left[VOA_{n_4/n_A}(H_2O)_{m_5}\right]^{(2-n_4)+} \overset{\text{solidification}}{\underset{\text{dissolution}}{\rightleftarrows}} VOA_{2/n_A}\cdot x_4H_2O \quad (2)$$

Table 4
Theoretical energy densities of VSSBs.

Counter ion	Active material					Energy density		
	Polarity	Compound	x	FW[a] (g (mol V)$^{-1}$)	($\times10^{-3}$ g C^{-1})	Composite ($\times10^{-3}$ g C^{-1})	[b] (mA cm^{-2})	[c] (W h kg^{-1})
Sulfate	Negative	$V(SO_4)_{1.5}\cdot xH_2O$	8.15 ± 0.13	341.73	3.54	5.93	46.7	70[e]–77[f]
	Positive	$VOSO_4\cdot xH_2O$	3.75 ± 0.05	230.5	2.39			
Chloride	Negative	$VCl_{1.5}\cdot xH_2O$	5[d]	194.115	2.01	4.37	63.3	95
	Positive	$VOCl_2\cdot xH_2O$		227.84	2.36			
Fluoride	Negative	$VF_{1.5}\cdot xH_2O$	5[d]	169.44	1.76	3.78	73.3	110
	Positive	$VOF_2\cdot xH_2O$		194.94	2.02			

[a] FW: formula weight.
[b] $F = 96{,}480$ C mol^{-1}, 0.277 (mA h C^{-1}) were used.
[c] Average voltage of the cell was assumed to be 1.5 V.
[d] The value was estimated because no literature value was found.
[e] Calculated for the obtained hydration number (x).
[f] Obtained energy density in this work. The value corresponds to reduced values (75%) according to the hydration number (x).

$$\begin{aligned} VA_{3/n_A}\cdot x_3H_2O &\overset{\text{dissolution}}{\underset{\text{solidification}}{\rightleftarrows}} [VA_{n_3/n_A}(H_2O)_{m_3}]^{(3-n_3)+} \\ &\overset{+e^-}{\underset{-e^-}{\rightleftarrows}} [VA_{n_2/n_A}(H_2O)_{m_2}]^{(2-n_2)+} \\ &\overset{\text{solidification}}{\underset{\text{dissolution}}{\rightleftarrows}} VA_{2/n_A}\cdot x_2H_2O \end{aligned} \quad (3)$$

Here, x_N is the number of hydrated water molecules in the hydrated salt of N-valent vanadium (A is the counteranion), n_N is the coordination number of the vanadium complex with an excess of counteranion A, and m_N is the hydration number of the complex.

Because the ratio of the active material to the liquid volume exceeds the solubility limit at least in the positive electrode, the battery works as shown in Fig. 10(b). Also, as shown in Fig. 10b′, the battery can work in the region where there is a high ratio of the active material to the volume of liquid. As shown in Fig. 11, the VSSB in (b) allows a dissolution-solidification equilibrium during charging and discharging, in contrast to the VRFB in (a) where only dissolved ions are present without precipitated solid. In the concentrated vanadium salt, many condensation and oxygenation reactions are anticipated. Four oxides, V_2O_5, VO_2, V_2O_3 and VO, are known [33]. For the positive electrode, the following reactions may be given:

$$2VO_2^+ + H_2O \rightleftarrows V_2O_5 + 2H^+ \quad (4)$$

$$2VO^{2+} + 2H_2O \rightleftarrows V_2O_4 + 4H^+ \quad (5)$$

Reaction (4) has been indicated in the literature [34]. These vanadium oxides have also been investigated [35] as anode or cathode materials in lithium-ion batteries [36]. Concerning the negative electrode, the divalent oxides, *e.g.*, vanadium monoxide VO, and trivalent oxides, including vanadium sesquioxide V_2O_3, have been investigated extensively [37]. Generally, equilibria involving these monoxide or sesquioxide species are investigated in solid-gas systems rather than aqueous systems [38]. However, because polyoxometalates [39] can form through substitution of protons with metal ions, the formation of some sulfate-based salt-oxide composite polyoxides is anticipated and further investigation of the vanadium chemistry should be performed to achieve a vanadium oxide battery with a high energy density.

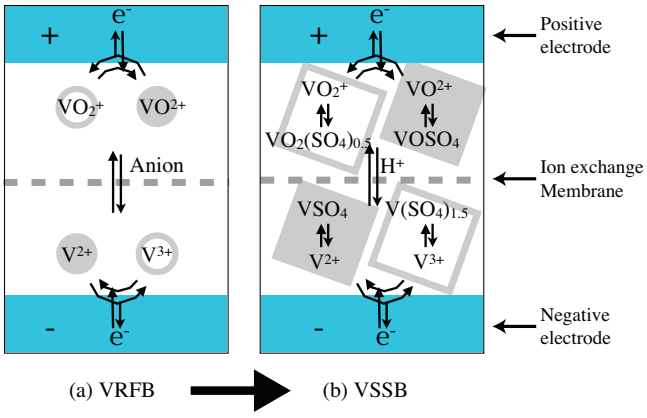

Fig. 11. Schematic of the charging and discharging process in a (a) VRFB and (b) VSSB. Hydrated water molecules are omitted. The horizontal dashed line indicates the ion-exchange membrane. Gray rectangles at the top and bottom indicate the positive and negative electrodes, respectively. Diamonds and circles indicate solid and dissolved species, respectively; filled and open symbols (diamonds and circles) indicate reduced and oxidized species, respectively.

3.5.3. Comparison of theoretical energy density

The theoretical energy density can be evaluated from the weight of active materials for the positive ($VOSO_4\cdot xH_2O$) and negative

Table 5
Performance of the optimized VSSB compared with those of other batteries.

Battery[a]	Cell voltage (V)	Volume energy density (W h L^{-1})	Weight energy density (W h kg^{-1})	Refs.
VSSB	1.34	300	70–110	This work
VRFB	1.3–1.5[b]	20–33	15–25	[13]
Lithium ion	4.0	500	200 (90[c]–120[d] [40])	[41]
Nickel–metal hydride	1.2	250	90	[41]
Lead acid	2.0	90	35	[41]
NaS	2.1	350	175	[41]

[a] VSSB: vanadium solid-salt battery, VRFB: vanadium redox-flow battery, NaS: sodium-sulfur battery.
[b] Refs. [15,24,25].
[c] The typical value for hybrid vehicles at present.
[d] The predicted requirement for plug-in hybrid vehicles in 2015.

($V(SO_4)_{1.5}\ xH_2O$) parts per mole of the materials. In the evaluation, the weight of the carbon materials was omitted because the mechanisms and effects of the carbon materials were not fully understood. Thus, there is a possibility that the weight of carbon materials can be reduced to a negligible amount. The number of hydrated water molecules in the sulfate salts was determined (Section 2.2). However, the number of hydrated water, chloride and fluoride molecules was estimated to be five, because insufficient information. The results of these calculations are summarized in Table 4. The energy density of 77 W h kg^{-1} obtained in this study exceeds the theoretical density corresponding to the determined hydration numbers (x_3 = 8.15 and x_4 = 3.75), probably because the hydration number changes depending on the conditions and materials used. The performance of the VSSB was also compared with those of other batteries (Table 5).

4. Conclusions

A VSSB containing solid-composites of $VOSO_4/(VO_2)_2SO_4$ and $VSO_4/V_2(SO_4)_3$ in its positive and negative half-cells, respectively, was developed. The Neosepta CMX C-1000 (cation-exchange membrane) and carbon felt XF30ADP14 (high electrical conductivity-type) were determined to optimize the energy density of the VSSB. An average EE and energy density of 87% and 77 W h kg^{-1}, respectively, were achieved at a current density of 5 mA cm^{-2}. The shape of the charging and discharging curves does not change after the second cycle, which revealed the excellent reversibility of the vanadium ions in the battery. The energy density was improved by evaporation of solutions containing the active materials, because of the effective redox reactions that occurred in the VSSB. These results suggest that the vanadium solid-salt battery has a sufficient energy density such that it could be used in electric vehicles or other mobile applications.

Acknowledgments

We thank Dr. T. Noguchi of Tohoku University; Prof. Y.P. Wu of Fudan University, Shanghai, China; Prof. K. Huang of Central South University, China; and Mr. M. Takahashi of the Experimental Facility for Alpha-Emitters from the Institute for Materials Research (IMR), Tohoku University for their helpful cooperation and discussions. We acknowledge Toyobo Co., Ltd., Japan, for supplying carbon felts and Asahi Glass Co., Ltd., Japan, for supplying membranes. This work was also performed at the International Research Center for Nuclear Materials Science, IMR, Tohoku University. This work was supported by a Grant-in-Aid for Scientific Research (B) (22360408).

References

[1] H. Karami, M.F. Mousavi, M. Shamsipur, S. Riahi, J. Power Sources 154 (2006) 298–307.
[2] H. Huang, T. Faulkner, J. Barker, M.Y. Saidi, J. Power Sources 189 (2009) 748–751.
[3] C. Yada, Y. Iriyama, T. Abe, K. Kikuchi, Z. Ogumi, Electrochem. Commun. 11 (2009) 413–416.
[4] U. S. D. o. t. I. U.S. Geological Survey, 2010.
[5] G. Wang, H. Zhang, L. Fu, B. Wang, Y. Wu, Electrochem. Commun. 9 (2007) 1873–1876.
[6] E. Sum, M. Rychcik, M. Skyllas-Kazacos, J. Power Sources 15 (1985) 179–190.
[7] E. Sum, M. Rychcik, M. Skyllas-Kazacos, J. Power Sources 16 (1985) 85.
[8] T. Yamamura, N. Watanabe, T. Yano, Y. Shiokawa, J. Electrochem. Soc. 152 (2005) A830–A836.
[9] G. Oriji, Y. Katayama, T. Miura, J. Power Sources 139 (2005) 321–324.
[10] C. de Leon, A. Frias-Ferrer, J. Gonzalez-Garcia, D. Szanto, F. Walsh, J. Power Sources 160 (2006) 716–732.
[11] M. Futamata, S. Higuchi, O. Nakamura, I. Ogino, Y. Takada, S. Okazaki, S. Ashimura, S. Takahashi, J. Power Sources 24 (1988) 137–155.
[12] P. Zhao, H. Zhang, H. Zhou, J. Chen, S. Gao, B. Yi, J. Power Sources 162 (2006) 1416–1420.
[13] M. Skyllas-Kazacos, G. Kazacos, G. Poon, H. Verseema, Int. J. Energy Res. 34 (2010) 182–189.
[14] D.R. Lide (Ed.), CRC Handbook of Chemistry and Physics on CD-ROM, Chapman&Hall, New York, 2000.
[15] M. Skyllas-Kazacos, M. Rychcik, R.G. Robins, A.G. Fane, M.A. Green, J. Electrochem. Soc. 133 (1986) 1057.
[16] K.R. Kneten, R.L. McCreery, Anal. Chem. 64 (1992) 2518–2524.
[17] S. Zhong, C. Padeste, M. Kazacos, M. Skyllas-Kazacos, J. Power Sources 45 (1993) 29–41.
[18] K.K. Cline, M.T. McDermott, R.L. McCreery, J. Phys. Chem. 98 (1994) 5314–5319.
[19] C.M. Hagg, M. Skyllas-Kazacos, J. Appl. Electrochem. 32 (2002) 1063–1069.
[20] P. Qian, H. Zhang, J. Chen, Y.H. Wen, Q. Luo, Z. Liu, D. You, B. Yi, J. Power Sources 175 (2008) 613–620.
[21] A. Sano, M. Kurihara, T. Abe, Z. Ogumi, J. Electrochem. Soc. 156 (2009) A682–A687.
[22] K. Matsuoka, S. Chiba, Y. Iriyama, T. Abe, M. Matsuoka, K. Kikuchi, Z. Ogumi, Thin Solid Films 516 (2008) 3309–3313.
[23] C. Jia, J. Liu, C. Yan, J. Power Sources 195 (2010) 4380–4383.
[24] M. Skyllas-Kazacos, F. Grossmith, J. Electrochem. Soc. 134 (1987) 2950–2953.
[25] M. Rychcik, M. Skyllas-Kazacos, J. Power Sources 22 (1988) 59–67.
[26] T. Mohammadi, M. Skyllas-Kazacos, J. Membr. Sci. 107 (1995) 35–45.
[27] T. Mohammadi, M.S. Kazacos, J. Power Sources 63 (1996) 179–186.
[28] Q. Luo, H. Zhang, J. Chen, D. You, C. Sun, Y. Zhang, J. Membr. Sci. 325 (2008) 553–558.
[29] B. Sun, M. Skyllas-Kazacos, Electrochim. Acta 37 (1992) 1253–1260.
[30] B. Sun, M. Skyllas-Kazacos, Electrochim. Acta 37 (1992) 2459–2465.
[31] X. Luo, Z. Lu, J. Xi, Z. Wu, W. Zhu, L. Chen, X. Qiu, J. Phys. Chem. B 109 (2005) 20310–20314.
[32] F. Rahman, M. Skyllas-Kazacos, J. Power Sources 72 (1998) 105–110.
[33] N.N. Greenwood, A. Earnshaw, Chemistry of the Elements, Elsevier, Amsterdam, 2005.
[34] F. Rahman, M. Skyllas-Kazacos, J. Power Sources 189 (2009) 1212–1219.
[35] V.N. Krasil'nikov, V.G. Bamburov, Doklady Chem. 416 (2007) 247–250.
[36] E. Shembel, R. Apostolova, V. Nagirny, D. Aurbach, B. Markovsky, J. Power Sources 81–82 (1999) 480–486.
[37] J. Stringer, J. Less-Common Metals 8 (1965) 1–14.
[38] J.O. Hill, I.G. Worsley, L.G. Hepler, Chem. Rev. 71 (1971) 127–137.
[39] G.M. Maksimov, Russ. Chem. Rev. 64 (1995) 445–461.
[40] T. a. I. Ministry of Economy, Tokyo, 2006.
[41] R.J. Brodd, in: J. Garche, C.K. Dyer, P.T. Moseley, Z. Ogumi, D.A.J. Rand, B. Scrosati (Eds.), Encyclopedia of Electrochemical Power Sources, vol. 1, Elsevier, Amsterdam, 2009, pp. 254–261.